Astron. Astrophys. 334, 592–598 (1998)

ASTRONOMY
AND
ASTROPHYSICS

A search for substellar companions around nine weak-lined T-Tauri stars with the Planetary Camera 2 of the Hubble Space Telescope⋆

Paola Sartoretti[1], **Robert A. Brown**[2], **David W. Latham**[3], **and Guillermo Torres**[3]

[1] Institut d' Astrophysique de Paris, 98 bis Boulevard Arago, F-75014 Paris, France
[2] Space Telescope Science Institute, 3700 San Martin Drive, Baltimore, MD 21218, USA
[3] Harvard-Smithsonian Center for Astrophysics, 60 Garden Street Cambridge, MA 02138, USA

Received 9 December 1997 / Accepted 24 February 1998

Abstract. To search for substellar companions, we have obtained I-band images of 9 weak-lined T-Tauri stars in the Taurus-Auriga star-forming region using the Planetary Camera 2 of the Hubble Space Telescope. Except for a stellar companion close to HBC 407, we found no companions within $8''$ of any of our targets. We did find 23 faint objects outside a separation of $8''$. For 12 of these, we have color information that implies they are background objects. Our sensitivity limit for companions separated by more than $1''$ is better than $\Delta I = 10$ mag. This limit degrades to $\Delta I = 5$ mag at a separation of about $0.2''$. For the median apparent magnitude, $I = 11$ mag, and median age, 10^7 yr, of our targets, the above sensitivity limits correspond to companions with 18 and 55 Jupiter masses, respectively.

To complement the imaging program, radial-velocity observations of the 9 stars were obtained using the Center for Astrophysics Digital Speedometers. There is a hint of a long-term acceleration of about 2 km s^{-1} over ten years in the radial velocity of HBC 407, consistent with the evidence for a close companion to HBC 407 found in the HST images. In addition, one of our targets, HBC 392 was found to be a double-lined spectroscopic binary.

Key words: stars: pre-main sequence – stars: imaging – stars: low-mass, brown dwarfs – planetary systems

1. Introduction

Substellar companions around solar-type stars are thought to form by at least two different mechanisms. Companions that form in the same way as binary stars, by the fragmentation of gravitationally unstable collapsing clouds (Larson 1978; Boss 1988; Pringle 1989), are called brown dwarfs (Stevenson 1991; Mazeh et al. 1997), while those that form by accretion in circumstellar disks of gas and dust (Lissauer & Stewart 1993; Podolak et al. 1993) are called planets.

The mass of a brown-dwarf fragment should be controlled by the Jeans mass, which reaches a minimum when the fragment becomes opaque, heats up, and can fragment no further. This qualitative limit is reached for fragments in the neighbourhood of a few Jupiter masses (M_J) (Boss 1996,1988). The upper limit for the mass of a planet is also only qualitatively understood (Boss 1996). Among other things, it may depend on the conditions in the disk, the total mass available, and whether large cores can grow soon enough to then capture the large mass of gas needed to make a giant planet before the gas dissipates (Zuckerman et al. 1995). Indeed, there may be a range of companion masses where these two formation mechanisms overlap. Because giant planets and brown dwarfs in this overlap region would have similar compositions, it would be difficult to distinguish them using observations of their spectra. A striking illustration of this point is the remarkable similarity between the spectra observed for Jupiter and for the brown-dwarf companion of Gliese 229 (Oppenheimer et al. 1995, Geballe et al. 1996).

The main factors controlling the luminosity emitted by substellar companions are their mass and age. Objects more massive than about 12 M_J may briefly burn deuterium, but all objects below the substellar limit of about 80 M_J radiate energy released by gravitational contraction and ultimately cool and and fade (Burrows et al. 1997). The main strategy of our search for substellar companions is to look for them around young stars, before they have had time to cool and grow too faint to be detected.

Because we use direct imaging, targets that are closer to us are better, since the angular separations would be larger. Unfortunately, there are very few young stars in the nearby field, and their ages are difficult to establish. For this reason, we have chosen to observe targets in the nearest star-forming region, Taurus-Auriga, where there are many stars younger than about 10^7 yr, when the ages of individual objects can be established reasonably well from their luminosities and spectral types. The main disadvantage of observing targets in Taurus-Auriga is the rather large distance, about 150 pc. Even with the superb resolution available with the Planetary Camera 2 (PC2) on the Hubble Space Telescope (HST), we are limited to projected separations larger than about 30 AU.

Send offprint requests to: P. Sartoretti,(sartoret@iap.fr)

⋆ Some of the observations reported here were obtained with the Multiple Mirror Telescope, a joint facility of the Smithsonian Institution and the University of Arizona

After solar-type protostars emerge from the clouds of gas and dust that enshrouded their birth, they collapse rapidly towards the main sequence in time scales of a few million years. During this classical T-Tauri star (cTTS) phase there are several manifestations of their youth, such as strong H_α emission and excess infrared emission from a circumstellar disk. This is the critical stage when planets may have the opportunity to form. However, it would be difficult to detect such planets due to the obscuration from the disk and its competing emission. For the targets of our search we have chosen weak-lined T-Tauri stars (wTTSs). We presume that these pre-main-sequence stars have recently cleared their circumstellar disks, as evidenced by their weak H_α emission and weak infrared excess.

In Sect. 2 we discuss the criteria used to select our targets and we present new spectroscopic results that help to characterize the targets. We summarize our HST observations and their reductions in Sect. 3, and discuss their use to search for companions in Sect. 4. The final section documents the wide companions that we found at separations larger than $8''$. All of the wide companions for which we have observed colors are consistent with being faint background objects.

2. Target selection and characteristics

For our original Cycle 4 HST proposal we selected 14 wTTS targets from the list of 53 wTTSs reported by Strom et al. (1989), their Table 1). We excluded wTTSs with large infrared excess, $\Delta K > 0.18$ mag, to avoid targets where the circumstellar disk has not yet cleared. We also excluded targets with known companions within $8''$ (Leinert et al. 1993).

Nine of our 14 proposed wTTS targets were ultimately observed with the PC2 on HST. These are listed in Table 1. Column (1) gives the number from the Herbig & Bell Catalog (1988, HBC) or TAP survey (Feigelson et al. 1987); (2) the right ascension and declination (B1950) from the Guide Star Catalog (we adopted B1950 rather than J2000 positions to allow easier cross-referencing with NTTS numbers); (3) and (4) the V and I_C magnitudes from Strom et al. (1989); (5) the I_J magnitude calculated from I_C using the transformations given by Holtzman et al. (1995); (6) and (7) the H_α equivalent width and infrared excess from Strom et al. (1989), except that the infrared excess, ΔK, has been converted from dex to magnitudes; (8) the spectral type from the HBC or TAP; (9) the log of the effective temperature corresponding to the spectral type, according to the calibration used by Kenyon & Hartmann (1995); (10) the log of the luminosity reported by Kenyon & Hartmann (1995), except that the luminosities for HBC 347 and TAP 51 were taken from Strom et al. (1989); and (11) the log of the age, estimated using the CMA evolutionary tracks from D'Antona & Mazzitelli (1994).

Fig. 1 shows our 9 targets plotted on a $\log T_{\rm eff}$ vs. $\log L$ HR diagram, along with evolutionary tracks. Four of our targets are younger than 10^7 yr, while two are quite young, about 10^6 yr old. On the other hand, four are older than 3×10^7 yr and have essentially reached the main sequence. In the case of HBC 392, which we discovered to be a double-lined spectroscopic binary

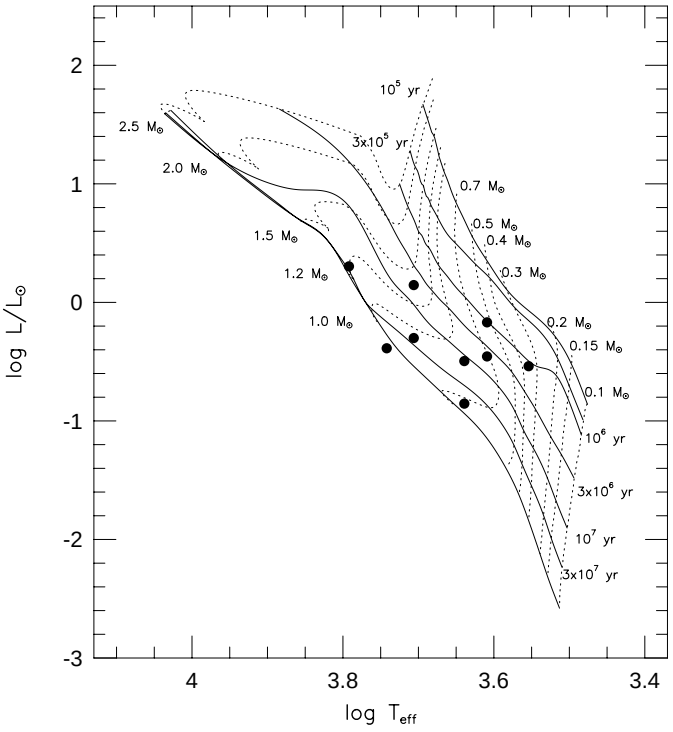

Fig. 1. The HR diagram for our 9 targets, plotted together with CMA evolutionary models and isochrones from D'Antona & Mazzitelli (1994).

(see below), we assumed that the total light was equally divided between the two components when we plotted it on the HR diagram and estimated its age.

To determine radial velocities, echelle spectra of all 9 of the wTTS targets were obtained with the CfA Digital Speedometers (Latham 1985,1992), primarily with the Multiple Mirror Telescope and 1.5-m Tillinghast Reflector at the Whipple Observatory on Mt. Hopkins, Arizona, but also with the 1.5-m Wyeth Reflector at the Oak Ridge Observatory in Harvard, Massachusetts. These observations cover a spectral window of about 45 Å centered near 5187 Å and reach typical signal-to-noise ratios of 10-25 per 8.3 km s^{-1} resolution element using photon-counting, intensified Reticon detectors. We used the cross-correlation package XCSAO (Kurtz et al. 1992) running inside the IRAF[1] environment for our velocity determinations. For the templates, we used theoretical spectra calculated by Jon Morse for a grid of Kurucz model atmospheres (1992a,b) spaced 250 K in $T_{\rm eff}$ and 10 km s^{-1} in $V \sin i$. We made educated guesses for the surface gravity to use for each star and adopted solar metallicity throughout. To determine the effective temperature, $T_{\rm eff}$, and rotational velocity, $V \sin i$, we ran grids of correlations for each star and chose the template that gave the best average value for the peak correlation. In the case of HBC 372 the average peak correlation occurred for the template with

[1] IRAF (Image Reduction and Analysis Facility) is distributed by the National Optical Astronomy Observatories, which are operated by the Association of Universities for Research in Astronomy, Inc., under contract with the National Science Foundation.

Table 1. The nine wTTSs observed with the PC2

Name	RA (B1950)	Dec	V (mag)	I_C (mag)	I_J (mag)	W(H_α) (Å)	ΔK (mag)	Sp	log($T_{\rm eff}$) (K)	logL_* ($L_\odot$)	log age yr
HBC 347	3:26:40.69	+24:20:22.0	12.05	11.01	10.89	0.2	$+0.08$	K1	3.708	-0.30	7.3
HBC 371	4:14:32.69	+28:25:42.0	13.56	11.33	11.03	4.0	$+0.03$	M2	3.544	-0.54	6.0
HBC 372	4:15:29.41	+16:51:31.5	13.26	11.99	11.84	4.0	$+0.10$	K5	3.639	-0.85	> 7.5
HBC 388	4:24:17.18	+17:44:01.7	10.34	9.45	9.31	0.5	$+0.00$	K1	3.706	$+0.15$	6.7
HBC 392	4:28:34.48	+17:00:01.3	12.53	11.15	10.99	0.2	$+0.13$	K5	3.639	-0.50	> 7.5
HBC 403	4:29:49.86	+17:56:38.4	13.22	11.37	11.13	0.7	-0.08	K7	3.609	-0.46	6.6
HBC 405	4:30:08.05	+24:27:26.5	12.21	10.50	10.18	3.0	$+0.18$	K7	3.609	-0.17	6.0
HBC 407	4:31:23.57	+18:23:54.6	12.67	11.43	11.29	0.3	-0.03	G8	3.742	-0.39	> 7.5
TAP 51	4:32:19.90	+18:15:27.4	10.95	9.98	9.87	1.3	-0.10	F8	3.792	$+0.30$	> 7.5

$V \sin i = 0$ km s^{-1}, and we have chosen not to interpolate for the rotational velocity of this star because we do not trust our ability to determine $V \sin i$ values smaller than about 5 km s^{-1}.

The results of our radial-velocity measurements with the CfA Digital Speedometers are summarized in Table 2. Columns (2) and (3) give the $T_{\rm eff}$ and log g adopted for the template spectra; (4) and (5) the number of observed spectra, N, and the span in days between the first and last observation; (6) the projected rotational velocity, $V \sin i$, derived from our spectra using a quadratic interpolation among the three templates centered on the one giving the best peak correlations; (7) and (8) the mean velocity, $V_{\rm ave}$, and standard deviation of the mean, σ; (9), (10), and (11) the external rms velocity residual, ext, the mean internal error estimate from XCSAO, int, and the ratio of the two, e/i; (12) the χ^2 of the velocities calculated using the individual internal error estimate from XCSAO for each observed velocity, (13) the probability that a star with constant velocity would have by accident a χ^2 larger than actually observed, $P(\chi^2)$; and (14) the average of the peak height of the correlation function, ht$_{\rm ave}$.

The extremely small value of $P(\chi^2)$ found for HBC 392 suggests that it has a variable velocity. Indeed, inspection of the one-dimensional correlation plots produced by XCSAO disclosed that one of the exposures of HBC 392 showed two well-separated peaks, while the other exposures showed hints of variation in the width of the correlation peak, as would be expected for blended spectra. Therefore, we analyzed the spectra for HBC 392 with the two-dimensional correlation scheme TODCOR (Zuckermann et al. 1995) as implemented at CfA. We first allowed the brightness ratio of the secondary to the primary, α, to be a free parameter in our TODCOR analysis. This stage of the analysis suggested that α is close to unity, which in turn suggests that the primary and secondary stars have similar spectra. Therefore, for the final TODCOR analysis we adopted the same template parameters for both stars ($T_{\rm eff} = 4500$ K, $V \sin i = 16$ km s^{-1}, log $g = 4.0$) and $\alpha = 0.68$. The $V_{\rm ave}$ reported for HBC 392 in Table 2 is the mean of the 11 pairs of TODCOR velocities, and the σ is the standard deviation of the mean of the pair averages.

The TODCOR velocities for our 11 exposures of HBC 392 are reported in Table 3. Column (1) gives the heliocentric Julian Date (-2,400,000), HJD, and (2) gives pairs of individual velocities for the two stars (but note that we have not been able to make reliable assignments of the individual velocities to the primary and secondary). The velocities derived using XCSAO for the other eight stars are also reported in Table 3.

HBC 407 also has a small value for $P(\chi^2)$, about 0.005, suggesting that this star may have a variable velocity. There is also a hint of a systematic drift with time for the velocity of this star, lending mild support to the suggestion that it may be a spectroscopic binary. The first 4 of the 5 velocity observations were obtained over a span of less than two years and cluster near 18.5 km s^{-1}, while the most recent observation comes after a gap of more than 7 years and is almost 2.5 km s^{-1} lower. The interpretation of this possible velocity drift is discussed below, in the context of our detection of a very close companion to HBC 407 with our HST images.

The average radial velocities reported in Table 2 can be used to check the membership of our HST targets in the Taurus-Auriga star-forming region. Neuhauser et al. (1995) consider a wTTS to be a bonafide kinematic member of Taurus-Auriga if the radial velocity is in the range 12 to 21 km s^{-1}. Seven of our 9 HST targets lie comfortably inside this velocity range. But, with a mean velocity of 3.4 ± 1.0 km s^{-1}, HBC 347 lies well outside the velocity range for Taurus-Auriga. It also lies a few degrees west of the region on the sky adopted for Taurus-Auriga by Leinert et al. (1993). With a mean velocity of 22.1 ± 0.3 km s^{-1}, TAP 51 lies just above the upper limit of the velocity range for Taurus-Auriga. Thus, HBC 347 and TAP 51 may not be bonafide members of Taurus-Auriga.

3. HST observations and data reduction

For our HST observations we chose the PC2 F785LP filter, which has a passband similar to the Johnson I_J filter, with a central wavelength near 870 nm and width of 130 nm (Biretta et al. 1996). The PC2 has a pixel spacing of $0.0455''$, and the point spread function (PSF) has a FWHM in the F785LP filter of $0.091''$.

For each of the stars we obtained frames at two spacecraft roll angles 20° apart to allow us to distinguish, by comparing the two frames, between PSF artifacts (which would appear at the same position in both images) and the signature of a companion

Table 2. Summary of the radial-velocity observations of the 9 wTTS targets obtained with the CfA Digital Speedometers

Name	Template $T_{\rm eff}$	log g	N	Span	$V \sin i$	$V_{\rm ave}$	σ	ext	int	e/i	χ^2	$P(\chi^2)$	ht$_{\rm ave}$
HBC 347	5000	4.0	6	3986	83.9	3.41	1.05	1.69	2.56	0.66	7.01	0.219573	0.714
HBC 371	4000	3.5	2	4015	41.7	16.32	3.32	4.70	2.77	1.70	3.02	0.082110	0.615
HBC 372	5250	4.5	5	740	0	15.94	0.25	0.20	0.56	0.35	0.45	0.978580	0.778
HBC 388	5000	3.5	6	2489	19.5	15.64	0.45	1.11	0.82	1.35	10.39	0.064956	0.838
HBC 392	4500	4.0	11	3230	10.0	17.07	0.40	4.18	1.17	3.53	59.99	0.000000	0.765
HBC 403	4250	3.5	5	733	5.3	18.31	0.25	0.55	0.53	1.04	3.76	0.439290	0.743
HBC 405	4250	3.5	7	2626	31.6	15.01	0.56	1.17	1.49	0.78	5.58	0.471338	0.753
HBC 407	5750	4.5	5	3285	8.0	17.93	0.56	1.26	0.72	1.74	14.71	0.005342	0.755
TAP 51	6500	4.0	7	2488	5.8	22.13	0.27	0.73	0.43	1.68	10.48	0.105800	0.843

Table 3. Individual radial-velocity determinations

HJD	$V_{\rm r}$	HJD	$V_{\rm r}$	HJD	$V_{\rm r}$
HBC 347		HBC 392		46449.76	17.89
46420.59	3.36	46421.72	11.98	46728.95	17.65
46426.64	3.21		24.72	47160.65	18.60
46449.68	3.56	46429.69	15.61		
46720.93	6.22		21.53	HBC 405	
50355.89	2.32	46493.53	14.05	47080.91	14.67
50406.75	1.31		17.67	47200.68	15.36
		46727.91	10.56	47494.75	15.80
HBC 371			20.43	47822.85	13.28
46391.74	13.16	46775.70	11.77	47901.60	16.81
50406.86	19.63		20.45	48201.87	15.39
		46804.67	12.26	49707.77	13.96
HBC 372			23.80		
46420.69	15.63	47162.78	11.88	HBC 407	
46430.64	16.04		23.15	46422.71	18.20
46449.74	15.92	47200.65	12.39	46429.65	17.82
46727.00	16.16		18.58	46775.76	19.30
47160.66	15.97	48872.93	11.34	47075.81	18.32
			26.70	49707.78	15.86
HBC 388		49262.99	37.98		
46421.71	15.15		-2.95	TAP 51	
46426.66	14.26	49651.99	15.12	46422.70	23.04
46727.91	16.29		16.59	46426.67	22.02
47078.87	16.72			46449.79	21.81
48258.59	14.62	HBC 403		46451.63	20.98
48910.79	16.81	46427.70	18.34	46728.84	22.46
		46432.68	19.01	47162.77	22.85
				48910.79	21.76

Table 4. Journal of HST Observations.

Name	Date (m/d/y)	Time (UT)	Exp (sec)
HBC 347a	1/02/95	18:06	70
HBC 347b	1/02/95	19:46	
HBC 371a	9/08/95	03:19	80
HBC 371b	9/08/95	19:23	
HBC 372a	9/03/95	17:20	60
HBC 372b	9/04/95	06:12	
HBC 388a	9/13/95	15:06	30
HBC 388b	9/14/95	13:37	
HBC 392a	9/05/95	20:41	80
HBC 392b	9/06/95	15:59	
HBC 403a	9/04/95	13:59	35
HBC 403b	9/05/95	12:30	
HBC 405a	22/1/96	15:55	40
HBC 405b	22/1/96	17:36	
HBC 407a	9/11/95	13:23	100
HBC 407b	9/11/95	14:59	
TAP 51a	9/04/95	07:33	26
TAP 51b	9/04/95	12:23	

(which would appear to rotate 20° between the two images). The frames obtained at the two roll angles are designated by a and b in Table 4. In frame a the position of north appears to be rotated 20° counterclockwise with respect to frame b.

With the goal of minimizing the amount of time wasted on overhead operations, we adopted a strategy of taking multiple exposures before reading out the CCD. We chose a pattern of nine exposures on a grid with about $8''$ separations. The PC2 shutter was closed during the spacecraft moves from one grid position to the next. (The amount of spacecraft time saved by this strategy was not significant.) One advantage of taking nine exposures in one frame was that we sampled the PSF at nine different positions, and could immediately recognize optical or CCD artifacts.

The individual exposure times were calculated to saturate the CCD in the central diffraction peak of the image, out to 3 pixels from the center of the image and not beyond. The goal was to improve the photon statistics in the wings of the image by giving away the central peak of the image, where detection of a faint companion is problematic in the first place. The exposure times, calculated for the magnitudes expected in the F755LP filter using the relation STMAG(F755LP)$= I_J + 1.52$, are given in Table 4, which is a journal of the observations.

For one of our faintest targets, HBC 403, the exposure time actually achieved was about half of the requested exposure time, and the exposure time for HBC 388 was accidently about twice as long as intended. Thus, the frames for these two objects allowed us to explore the effects on the PSF of images which are

over- and under-exposed by about a factor of two compared to the other seven targets.

The data were reduced and geometrically corrected using standard HST pipeline processing. From each frame, we extracted nine $8'' \times 8''$ sub-images centered on the stellar images. We registered the sub-images using both a sub-pixel cross-correlation, and the IRAF task "imcentroid". The results of these two independent approaches agreed within 0.1 pixels. We removed cosmic rays (using IRAF "imcombine") and averaged each set of 9 sub-images obtained with the same telescope roll angle to obtain two images per star, which we call image a and image b, differing by the 20° rotation.

4. Search for companions

Because the images were saturated within 3 pixels from the center, any companion inside that separation ($0.137''$) was neither well resolved nor easily recognized. Nevertheless, we have searched for possible companions with less than 3 pixel separations by examining the radial profiles for broadening outside the saturated region. For this purpose, we averaged images a and b, excluding the saturated pixels. Then we compared the azimuthally averaged radial profile of each star with theoretical profiles, which were constructed using the Tiny Tim HST PSF generation package (Krist 1994) for the F785LP filter bandpass and the 9 positions on the CCD corresponding to our observations.

In Fig. 2 are plotted the azimuthally averaged radial profiles of all the observed star images. The radial profile of the model PSF, plotted as a solid line, shows what would have been expected in absence of CCD saturation. The error bars are the 1-σ PSF variations at the 9 field positions. For clarity we only plotted observed points that differ by more than 1σ from the model PSF. Except for HBC 403, which was underexposed, saturation is important inside $\sim 0.18''$. Outside $\sim 0.23''$, the profiles of HBC 347, 371, 372, 392, 403 and 405 are all consistent within 1σ with the theoretical single-star profile. The profile of HBC 407 is $\sim 9\sigma$ higher than the theoretical PSF at $0.23''$, $\sim 4\sigma$ higher at $0.27''$, and $\sim 1.8\sigma$ higher at $0.32''$. This suggests the presence of an unresolved companion to HBC 407.

The a and b images for HBC 407 are shown in Fig. 3 (bottom) with the theoretical PSF subtracted and the saturated region inside 4 pixels ($0.18''$) excluded. The presence of the companion and its rotation of 20° between spacecraft roll angles is evident. Model 1 is a simulated binary system with separation of 4 pixels ($0.18''$) and $\Delta I = 2.7$ mag; Model 2 has a separation of 3 pixels ($0.135''$) and $\Delta I = 1.7$ mag. By performing a series of such simulations to explore the effects of separation and magnitude difference, we estimate for the companion of HBC 407 a separation of $0.14 \pm 0.02''$ and $\Delta I = 1.7 \pm 0.5$ mag at a position angle of $48^\circ \pm 10^\circ$ at the epoch of our observations, 1995.86. The hint in our radial velocity data for a slow drift of perhaps 2 km s^{-1} over 10 years is not inconsistent with a companion in orbit around HBC 407. For example, a companion in a circular orbit with radius 21 AU (corresponding to $0.14''$ separation at 150 pc) and companion mass nearly equal to that of the primary would have a period of 60 years and orbital amplitude of 6 km s^{-1}.

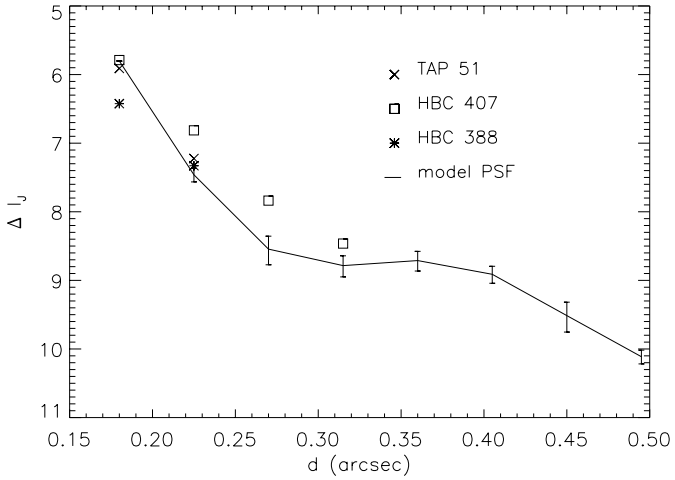

Fig. 2. Azimuthally averaged radial profiles observed for our targets (points) and our model PSF (dashed line). Only points that deviate from the theoretical PSF by more than 1σ are plotted.

Based on simulations of the type described for HBC 407, we established the following detection limits for close "unresolved" companions to our other 8 targets. At a separation of 3 pixels ($0.137''$) there were no other companions with $\Delta I < 2$, and none with $\Delta I < 3$ mag at 4 pixels.

For wider separations our search technique consisted of examining difference images — both the subtraction of the two composite data images (a and b), where a companion should display positive and negative signatures 20° apart, and also the subtraction of theoretical PSFs matched to the separate a and b images. We found no candidate companions out to separations of $8''$. We inserted artificial companions into the images at various separations, position angles, and magnitude differences to explore and characterize our detection limits. These limits are illustrated in Fig. 4 Our sensitivity limit for companions separated by more than $1''$ is better than $\Delta I = 10$ mag. This limit degrades to $\Delta I = 5$ mag at a separation of about $0.2''$.

The brightness of a substellar companion depends both on the mass and the age. Table 5 lists the photometric detection limits for companions at projected separations of 30 AU ($0.2''$) and 150 AU ($1''$) from the target stars. Also indicated are the corresponding masses, kindly computed for us by D. Saumon (private communication) using an updated version of the Saumon et al. (1996) brown dwarf model, which includes the effects of molecular opacities and is appropriate for substellar objects with masses $\geq 10 M_J$. We have not applied this analysis to the four stars closest to the main sequence because their ages are old and not well determined.

5. Faint sources in the field of view

We searched our HST images for faint sources in the field of view and identified 23 such sources, all with angular separations larger than $8''$. It is not surprising that we did not detect any faint

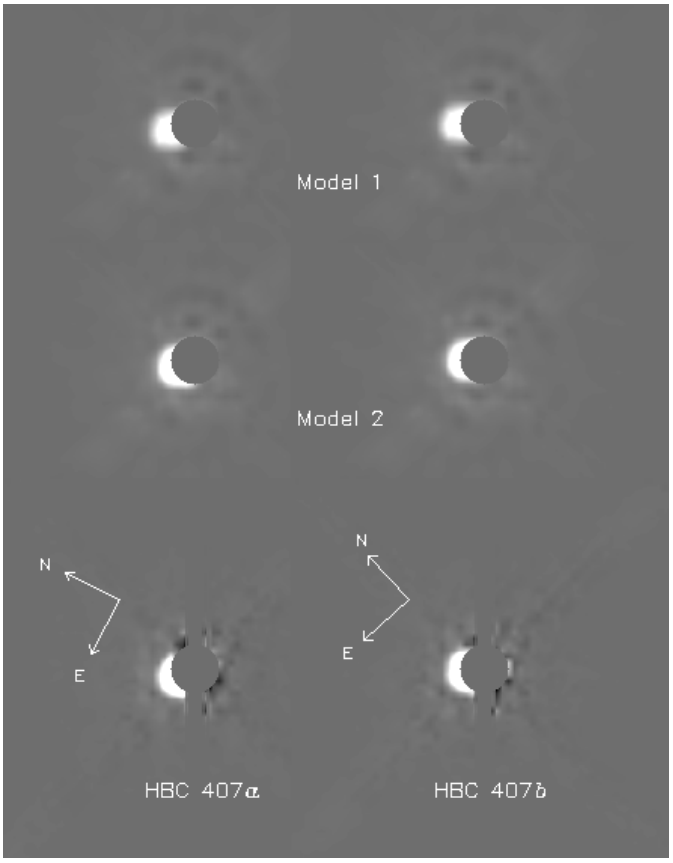

Fig. 3. In the bottom panel are shown HBC $407a$ and HBC $407b$ with the theoretical PSF subtracted. The presence of the close companion and its apparent rotation with the spacecraft roll angle is evident. Model 2, in the middle panel, shows our best representation of the binary system HBC 407, and has $d \sim 0.135''$ and $\Delta I \sim 1.7$ mag. Model 1, in the top panel, has $d \sim 0.18''$ and $\Delta I \sim 2.7$.

Table 5. Detection limits for companions at projected separations of 30 AU and 150 AU from the target stars. M_I is the absolute magnitude in the I_J band, and M_J is the mass in units of the Jupiter mass.

	log age	Sep 30 AU		Sep 150 AU	
	yr	M_I	M_J	M_I	M_J
HBC 347	7.3	10.12	90	15.62	15
HBC 371	6.0	10.45	40	15.95	<10
HBC 388	6.7	7.42	90	12.92	20
HBC 403	6.6	10.25	45	15.65	<10
HBC 405	6.0	9.30	60	14.70	<10

sources with separations inside $8''$, because one of our selection criteria was that our targets should have no known companions inside that separation. We used IRAF tools to measure the I_J magnitudes inside apertures $1''$ in diameter. For the fainter sources the errors in our I_J magnitudes are dominated by the photon statistics, but for the brighter sources the systematic errors in the transformation from counts to I_J are also important. The uncertainties in I_J range from ~ 0.07 to ~ 0.15 mag.

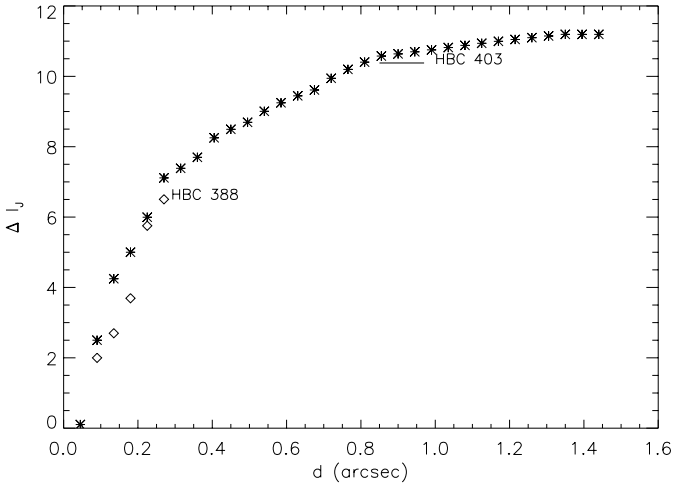

Fig. 4. Detection limits for companions as a function of angular separation from the target star. The detection limits for HBC 388 are somewhat poorer at small separations because of the heavier exposures and higher level of saturation in those images. The detection limits for HBC 403 are poorer at large separations because of the lighter exposures in those images.

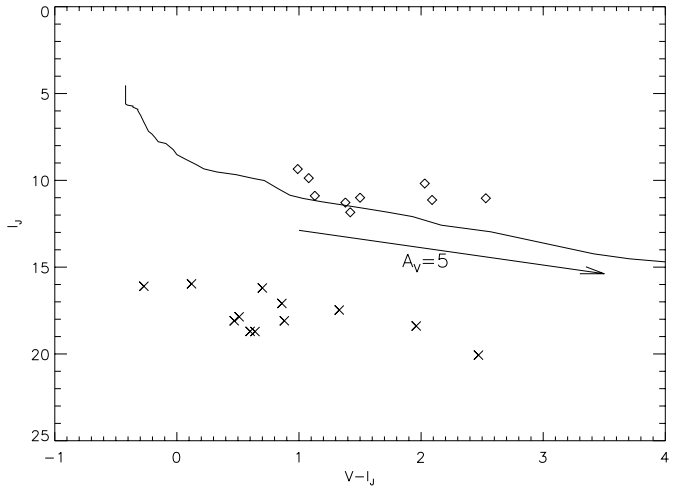

Fig. 5. I_J versus $V - I_J$ colour-magnitude diagram. The field sources are plotted as crosses, the wTTS targets as squares. The observed main sequence (Johnson 1965) is plotted as a line, and the reddening vector for $A_V = 5$ is shown

We were able to identify some of the field sources on the Digital Sky Survey (DSS). For these sources we estimated the V magnitudes using the DSS calibration (Doggett et al. 1996) and adopting a linear extrapolation for stars fainter than $V = 16$ mag. Unfortunately, the uncertainties in these V-magnitude estimates are large, at least ± 0.5 mag. Table 6 lists the field sources that we identified, together with the angular separations, position angles (measured eastward from north), and magnitude estimates. An entry of *nr* in the V column indicates that the source was not resolved on the DSS.

HBC 371 C_1/C_2, and HBC 403 B_1/B_2 are probably binaries, because of their small separations and similar magnitudes. HBC 347 B appears too diffuse to be a star.

Table 6. Faint sources in the field of view

Field Source	Sep ($''$)	P.A. ($^\circ$)	V	I_J
HBC 347 B	12.42	267.8	19.1	18.7
HBC 347 C	17.96	326.6	20.1	18.4
HBC 347 D	23.89	187.2	18.4	18.1
HBC 371 B	18.24	289.7	-	19.1
HBC 371 C_1	14.75	118.2	-	19.2
HBC 371 C_2	14.27	118.4	-	19.4
HBC 392 B	23.81	265	19.3	18.7
HBC 392 C	8.83	48	-	21.0
HBC 392 D	18.73	237	22.4	20.1
HBC 403 B_1	23.95	1	19	18.1
HBC 403 B_2	23.94	2.5	*nr*	19.4
HBC 403 C	21.44	95	17.9	17.1
HBC 403 E	16.17	170	-	19.9
HBC 403 D	28.62	87	18.8	17.5
HBC 405 B	11.16	58	16.9	16.2
HBC 405 C	6.95	300.1	-	17.7
HBC 405 D	11.91	100.5	-	20.2
HBC 407 B	0.13	48	*nr*	13.0
HBC 407 C	22.82	149	18.37	17.9
HBC 407 D	24.71	216.4	-	18.8
HBC 407 E	9.83	301.4	-	21.2
TAP 51 B	22.41	322	15.8	16.1
TAP 51 C	25.79	258.5	16.1	16.0

The field stars for which we have V-magnitude estimates are plotted on an I_J vs $V - I_J$ colour-magnitude diagram in Fig. 5, together with our wTTS targets. We have set the zero point of the magnitude scale to correspond to the distance of Taurus-Auriga, 150 pc. The observed main sequence (Johnson 1965) and a reddening vector for $A_V = 5$ mag are also plotted. All the field sources lie well below the main sequence, consistent with the interpretation that they are background objects.

Acknowledgements. Many thanks to Didier Saumon for providing us the I magnitude to mass conversion and to Roberto Gilmozzi and Stefano Casertano for helpful suggestions on the data acquisition strategy and on the data calibration. PS is an ESA fellow. Part of this work was supported by NASA grant. The files of the DSS we used are copyright (c) 1994, Association of Universities for research in Astronomy. This work has made use of the Simbad database, operated at the CDS, Strasbourg, France.

References

Biretta J.A., Burrows C., Holtzman J., et al., 1996, WFPC2 Instrument Handbook version 4. STScI, Baltimore
Boss A.P., 1988, ApJ 331, 370
Boss A.P., 1996, Nat 379, 397
Burrows A., Marley W., Hubbard W.B., et al., 1997, ApJ, in press
D'Antona F., Mazzitelli I., 1994, ApJS 90, 467
Doggett, J., Postman, M., Lasker, B.M., Meakes, M., 1996, Astronomical Data Analysis Software and System V, A.S.P. Conf. Series, 101, 159
Feigelson E.D., Jackson J.M., Mathieu R.D., et al., 1987, AJ 94, 1251 (TAP)
Geballe T.R., Kulkarni S.R., Woodward C.E., et al., 1996, ApJ 467, L101
Herbig G.H., Bell K.R., 1988, Lick Obs. Bull. No. 1111 (HBC)
Holtzman J.A., Burrows C.J., Casertano S., et al., 1995, PASP 107, 1065
Johnson H.L., 1965, ARA&A 4, 193
Kenyon S.J., Hartmann L.W., 1995, ApJS 101, 117
Krist J., 1994, Tiny Tim User's Manual, version 4. STScI, Baltimore
Kurtz M.J., Mink D.J., Wyatt W.F., et al., 1992, in: Worrall D.M., Biemesderfer C., Barnes J. (eds.), Astronomical Data Analysis Software and Systems I, ASPC 25, p. 432
Kurucz R.L., 1992a. In: Barbuy B., Renzini A. (eds.) IAU Symposium 149, The Stellar Population of Galaxies. Kluwer, Dordrecht, p. 225
Kurucz R.L., 1992b, Rev. Mex. Astron. Astrofis. 23, 187
Larson R.B., 1978, MNRAS 184, 69
Leinert C., Zinnecker H., Weitzel N., et al. 1993, A&A 278, 129
Lissauer J.J., Stewart G.R., 1993. In: Levy E.H., Lunine, J.I. (eds.) Protostars and Planets III. Univ. Arizona Press, Tucson, p. 1061
Latham D.W., 1985. In: Philip A.G.D, Latham D.W. (eds.) IAU Coll. 88, Stellar Radial Velocities. L. Davis Press, Schenectady, p. 21
Latham D.W., 1992. In: McAlister H.A., Hartkopf W.I. (eds.) IAU Coll. 135, Complementary Approaches to Binary and Multiple Star Research, PASPC 32, 110
Mazeh T., Mayor M., Latham D.W., 1997, ApJ 478, 367
Neuhäuser R., Sterzik M.F.,Torres G., et al. 1995, A&A 299, L13
Oppenheimer B.R., Kulkarni S.R., Matthews K., et al., 1996, Sci 270, 147
Podolak M., Hubbard W.B., Stern S.A., 1993. In: Levy E.H., Lunine J.I. (eds.) Protostars and Planets III. Univ. Arizona Press, Tucson, p. 1109
Pringle J.E., 1989, MNRAS 239, 361
Saumon D., Hubbard W.B., Burrows A., et al., 1996 ApJ, 460, 993
Stevenson D.J., 1991, ARA&A 29, 163
Strom K.M., Strom S.E., Edwards S., et al., 1989, AJ 97, 1451
Zuckerman B., Forveille T., Kastner J.H. 1995, Nat 373, 494